Eur Biophys J (1994) 23:29–38

European Biophysics Journal

Statistics of RNA melting kinetics

Manfred Tacker [1], Walter Fontana [2], Peter F. Stadler [1, 2], Peter Schuster [1, 2, 3]

[1] Institut für Theoretische Chemie, Universität Wien, Währingerstrasse 17, A-1090 Wien, Austria
[2] Santa Fe Institute, 1660 Old Pecos Trail, Santa Fe, NM 87501, USA
[3] Institut für Molekulare Biotechnologie, Postfach 100813, D-07708 Jena, Germany

Received: 5 July 1993 / Accepted: 22 November 1993

Abstract. We present and study the behavior of a simple kinetic model for the melting of RNA secondary structures, given that those structures are known. The model is then used as a map that assigns structure dependent overall rate constants of melting (or refolding) to a sequence. This induces a "landscape" of reaction rates, or activation energies, over the space of sequences with fixed length. We study the distribution and the correlation structure of these activation energies.

Key words: Activation energy landscape – RNA folding – RNA melting – RNA secondary structure

1. Introduction

Single stranded RNA sequences fold into complex three-dimensional structures. A tractable, yet reasonable, model for the map from sequences to structures considers a more coarse grained level of resolution known as the secondary structure. The secondary structure is a list of base pairs such that no pairings occur between bases located in different loop regions. Algorithms based on empirical energy data have been developed to compute the minimum free energy secondary structure of an RNA sequence (Zuker and Stiegler 1981; Zuker and Sankoff 1984).

The structure influences a variety of biophysical quantities such as, for example, kinetic rate constants of melting. The situation is a composition of two mappings: a folding map that assigns a structure to a sequence, and a second map that assigns some biophysical property to the structure. By "landscape" we refer to the graph of this composite mapping that assigns to each sequence a scalar that quantifies some property based on the structure attained by the sequence.

Systematic studies on RNA landscapes (Fontana et al. 1991; 1993 a, b; Bonhoeffer et al. 1993) were encouraged by the recent interest in statistical properties of randomly assembled RNA molecules which are used by several experimental techniques in applied molecular evolution (Horowitz et al. 1989; Joyce 1989; Tuerk and Gold 1990; Ellington and Szostak 1990; Beaudry and Joyce 1992). The only class of value landscapes that is presently accessible to extensive computer explorations is derived from RNA secondary structures (Fontana et al. 1991, 1993 a, b). In this case fairly reliable prediction algorithms are available (Jaeger et al. 1989; Zuker 1989). Computations of RNA tertiary structures or protein structures are both too expensive and not sufficiently accurate to allow systematic studies.

In recent work we have investigated essentially two kinds of landscapes: the scalar landscape of the free energy of folding, and the non-scalar landscape of the minimum free energy secondary structures themselves (Fontana et al. 1991, 1993 a, b). In this contribution we look into a further biophysical property that is mediated by the structure: the kinetics of melting. To this end we build a very simple kinetic model of melting (and, conversely, re-folding) of RNA secondary structures. The model is then used as a specification to compute, for any given sequence, overall rate constants of melting and structure formation, or, equivalently, to compute the corresponding activation energies. It is the landscape of these rates, more precisely: of the activation energies, that we investigate in this paper. It follows, in principle, the same generic concept mentioned recently in a short note (Fernández and Shakhnovich 1990), in which, however, no explicit sequence dependence was discussed.

We also consider three different alphabets: the binary GC alphabet, the biophysical AUGC alphabet and the synthetic GCXK alphabet. A, U, G and C denote the naturally occurring bases adenine, uracil, guanine and cytosine. K and X are abbreviations for 3-β-D-ribofuranosyl-(2,6-diaminopyrimidine) and xanthosine, a derivative of purine. The basic pair between K and X has roughly the same energy as the base pair between G and C (Piccirilli et al. 1990). Owing to the lack of experimental data we used the GC parameter set for XK. The synthetic

Correspondence to: P. Schuster

GCXK alphabet represents an alphabet with two equally strong base pairs. It is of particular interest since it allows one to study the effects of two base pairs versus one base pair (GC) without obscuring the results by the additional influence of different base pair strength and (GU) base pairing as in the natural AUGC alphabet.

2. RNA melting kinetics

2.1. A model for melting RNA secondary structures

An RNA secondary structure is a list of base pairs (i, j) with $i < j$ and satisfying two conditions: (1) each base is involved in at most one pairing interaction, and (2) if (i, j) and (k, l) are pairs, then $i < k < l < j$ or $k < i < j < l$ (Waterman and Smith 1978). Such a list can be visualized as a planar graph with two major structural elements: loops, or unpaired regions, and stacks of contiguous base pairs, also referred to as stacks. Condition (2) states that bases within a loop cannot pair with bases outside that loop. Secondary structures can be assigned free energies by summing up the (measured) energy contributions from their constituent loops and stacks. In the following the term "secondary structure" refers to the minimum free energy secondary structure.

Melting of RNA secondary structures is considered as an "all-or-none" process in the sense that only the completely folded minimum free energy secondary structure, S, and the open chain, C, are assumed to be present at measurable concentrations. According to the common stationarity assumption of chemical reaction kinetics the concentrations of all intermediates are considered as small and constant in time. The over-all process is then described by the following reaction equation:

$$\mathrm{C} \underset{k_D}{\overset{k_R}{\rightleftarrows}} \mathrm{S} \tag{1}$$

Consistent with the current biophysical literature (Pörschke 1974) we use the terms "recombination" rate constant, k_R, and "dissociation" rate constant, k_D, when referring to the refolding and melting process, respectively. These terms were originally used in studies of double helix formation from separate RNA strands (Pörschke and Eigen 1971; Pörschke 1971).

Consider a minimum free energy secondary structure S consisting of n double helical stacks denoted by η_1, $\eta_2, \ldots \eta_n$. We obtain S from a sequence by using a variant of the Zuker-Stiegler algorithm (Zuker and Stiegler 1981; Zuker and Sankoff 1984). We further assume that the stacks η_i, $i = 1, \ldots, n$, form and melt independently of one another, and that the only intermediates between C and S are the partially folded structures containing any of the stacks η_i. We do not consider intermediates consisting of other structural elements. Accordingly, all intermediates

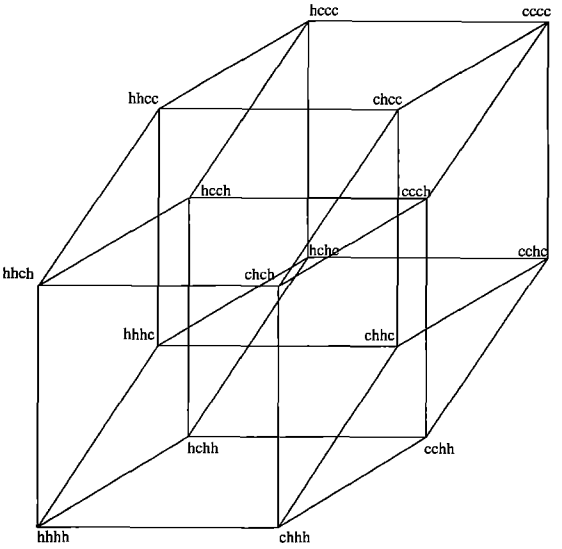

Fig. 1. Stepwise formation and melting of an RNA secondary structure consisting of four helical regions. The unfolded molecule, C, the completed secondary structure, S, and all intermediates are represented by the corners of a hypercube. Edges correspond to reversible reactions involving the formation and the melting of a single stack

are encoded as a binary string $(s_1, s_2 \ldots s_n)$ of length n with $s_i = \mathrm{h}$ or $s_i = \mathrm{c}$ indicating whether the ith stacking region is in double helical form or in the molten state, respectively. The complete secondary structure S is expressed as (hhh ... h), and the open chain C is represented by (ccc ... c). The system, therefore, consists of 2^n different states: S, C and the $2^n - 2$ intermediates encoded as

$$\begin{array}{llll} \mathrm{H}_1 = (\mathrm{hcc} \ldots \mathrm{c}) & \mathrm{H}_2 = (\mathrm{chc} \ldots \mathrm{c}) & \ldots & \mathrm{H}_n = (\mathrm{cc} \ldots \mathrm{ch}) \\ \mathrm{H}_{12} = (\mathrm{hhc} \ldots \mathrm{c}) & \mathrm{H}_{13} = (\mathrm{hchc} \ldots \mathrm{c}) & \ldots & \mathrm{H}_{n-1,n} = (\mathrm{c} \ldots \mathrm{chh}) \\ \vdots & & \ldots & \vdots \\ \mathrm{H}_{12\ldots n-1} = (\mathrm{hh} \ldots \mathrm{hc}) & \mathrm{H}_{13\ldots n} = (\mathrm{hch} \ldots \mathrm{h}) & \ldots & \mathrm{H}_{23\ldots n} = (\mathrm{chh} \ldots \mathrm{h}) \end{array}$$

We retain the symbols $\mathrm{C} \equiv \mathrm{H}_0$ for the open chain and $\mathrm{S} \equiv \mathrm{H}_{12\ldots n}$ for the folded molecule. The individual structures can be thought of as occupying the corners of a Boolean hypercube of dimension n (Fig. 1).

Expressions for overall interconversion $\mathrm{C} \rightleftharpoons \mathrm{S}$ can be derived from the general reaction mechanism which allows for interconversion of any two species. The kinetic equations are given by $[\mathrm{C}] = c$, $[\mathrm{H}] = h$ and $[\mathrm{H}_\mu] = h_\mu$, $(\mu = 1, 2, \ldots, 23 \ldots n)$. Let $k_{\mu\varrho}$ be the (first order) rate constant for the conversion of the intermediate μ into ϱ

$$\begin{aligned} \dot{c} &= \sum_{\varrho} (k_{\varrho \mathrm{C}} h_\varrho - k_{\mathrm{C}\varrho} c) \\ \dot{h}_\mu &= \sum_{\varrho \neq \mathrm{C,S}} (k_{\varrho\mu} h_\varrho - k_{\mu\varrho} h_\mu) - (k_{\mu \mathrm{C}} + k_{\mu \mathrm{S}}) h_\mu + k_{\mathrm{C}\mu} c + k_{\mathrm{S}\mu} s, \\ \dot{s} &= \sum_{\varrho} (k_{\varrho \mathrm{S}} h_\varrho - k_{\mathrm{S}\varrho} s) \end{aligned} \tag{2}$$

with $k_{\mu\mu=0}$. This may be rewritten in matrix form as

$$\dot{\boldsymbol{h}} = (-A) \cdot \boldsymbol{h} + c \cdot \boldsymbol{p} + s \cdot \boldsymbol{q}, \tag{3}$$

where $\boldsymbol{h} = (h_\mu)$ is the concentration vector of the intermediates, $\boldsymbol{p}$ is the vector of the $k_{\mathrm{C}\mu}$, $\boldsymbol{p} = (k_{\mathrm{C}1}, \ldots, k_{\mathrm{C}12\ldots n-1})$

and $\boldsymbol{q} = (k_{S1}, \ldots, k_{S12\ldots n-1})$. The matrix entries of A are given by

$$\alpha_{\mu\varrho} = -k_{\varrho\mu} + \left[\sum_{\tau} k_{\mu\tau} + k_{\mu C} + k_{\mu S}\right] \delta_{\varrho\mu}, \tag{4}$$

The steady state assumption for intermediates,

$$\dot{h}_\mu = 0 \quad \forall \mu \neq C, S \tag{5}$$

allows one to compute the stationary concentrations $\bar{h}_k$ of all partially folded structures from the system of linear equations:

$$A \cdot \bar{h} = c \cdot \boldsymbol{p} + s \cdot \boldsymbol{q}. \tag{6}$$

If the system of monomolecular reactions is strongly connected, that is: if there is a reaction pathway with positive rate constants between any two species, then A is invertible, and the concentrations of the intermediates are uniquely determined by

$$\bar{h} = (A^{-1}\boldsymbol{p})\, c + (A^{-1}\boldsymbol{q})\, s. \tag{7}$$

This is also an immediate consequence of Feinberg's deficiency 0 theorem (Feinberg 1977). From the equation for c,

$$\dot{c} = k_D \cdot s - k_R \cdot c = \sum_{\mu \neq C,S} k_{\mu C} \bar{h}_\mu - \sum_{\mu \neq C,S} k_{C\mu} c + k_{SC} s - k_{CS} c,$$

we obtain the explicit expressions for the overall rate constants as

$$\begin{aligned} k_R &= \mathbf{1}\boldsymbol{p} + k_{CS} - \boldsymbol{k}_c A^{-1} \boldsymbol{p} \\ k_D &= \boldsymbol{k}_c A^{-1} \boldsymbol{q} + k_{SC} \end{aligned} \tag{8}$$

where $\boldsymbol{k}_c$ is the vector $k_{\mu C}$ and $\mathbf{1}$ is the vector $(1, \ldots, 1)$.

2.2. Sequential melting

The case of sequential folding and melting of the secondary structure S along an unbranched dominant path

$$C \underset{k_{10}}{\overset{k_{01}}{\rightleftharpoons}} H_1 \underset{k_{21}}{\overset{k_{12}}{\rightleftharpoons}} H_{01} \underset{k_{32}}{\overset{k_{23}}{\rightleftharpoons}} H_{123} \underset{k_{43}}{\overset{k_{34}}{\rightleftharpoons}} \cdots \underset{k_{m-1,m-2}}{\overset{k_{m-2,m-1}}{\rightleftharpoons}} H_{12\ldots m-1} \underset{k_{m,m-1}}{\overset{k_{m-1,m}}{\rightleftharpoons}} S \tag{9}$$

can be readily solved analytically. The intermediates are ordered along this path such that the stack η_1 forms most easily, η_2 is the next most likely, etc. Formation of the stack η_m is least likely. Equivalently, the stack η_m melts most easily, etc. All other intermediates except the $m-1$ explicitly shown in the reaction scheme (9) are neglected.

Let us now denote the concentrations of the intermediates by: $[H_1] = h_1$, $[H_{12}] = h_2, \ldots$, $[H_{12\ldots m-1}] = h_{m-1}$, $[C] = c$ and $[S] = s$. The kinetic equations are straightforward:

$$\begin{aligned} \dot{c}_1 &= -k_{01} c + k_{10} h_1 \\ \dot{h}_1 &= k_{01} c - (k_{10} + k_{12}) h_1 + k_{21} h_2 \\ \dot{h}_2 &= k_{12} h_1 - (k_{21} + k_{23}) h_2 + k_{32} h_3 \\ &\vdots \\ \dot{h}_{m-1} &= k_{m-2,m-1} h_{m-2} - (k_{m-1,m-2} + k_{m-1,m}) h_{m-1} + k_{m,m-1} s \\ \dot{s} &= -k_{m,m-1} s + k_{m-1,m} h_{m-1}. \end{aligned} \tag{10}$$

The matrix A in Eq. (3) becomes

$$A = \begin{pmatrix} k_{10}+k_{12} & -k_{21} & 0 & \ldots & 0 \\ -k_{12} & k_{21}+k_{23} & -k_{32} & \ldots & 0 \\ 0 & -k_{23} & k_{32}+k_{34} & \ldots & 0 \\ 0 & 0 & -k_{34} & \ldots & 0 \\ \vdots & \vdots & \vdots & \ddots & \vdots \\ 0 & 0 & 0 & \ldots & -k_{m-1,m-2} \\ 0 & 0 & 0 & \ldots & k_{m-1,m-2}+k_{m-1,m} \end{pmatrix} \tag{11}$$

and the vectors $\boldsymbol{p}$ and $\boldsymbol{q}$ have only one non-zero component $p_1 = k_{C1}$ and $q_m = k_{S,m-1}$. The overall rate constants results as

$$\begin{aligned} k_R &= \frac{k_{01} \cdot k_{12} \cdot \ldots \cdot k_{m-1,m}}{|A|}, \\ k_D &= \frac{k_{10} \cdot k_{21} \cdot \ldots \cdot k_{m,m-1}}{|A|}. \end{aligned} \tag{12}$$

As a consequence of the assumption of independent substructure formation the overall equilibrium constant factorizes into equilibrium constants for individual stacks:

$$K = \frac{k_R}{k_D} = \frac{k_{01}}{k_{10}} \cdot \frac{k_{12}}{k_{21}} \cdot \ldots \cdot \frac{k_{m-1,m}}{k_{m,m-1}}. \tag{13}$$

We shall make use of this fact in the computation of individual rate constants.

2.3. Hypercubic melting

It is reasonable to assume that the only allowed reversible reactions are those that involve structures differing in the state of one stack. The total reaction network is then given by the edges of an n dimensional hypercube, that is: all $k_{\mu\varrho}$ in Eq. (2) are zero except for intermediates whose binary encodings have Hamming distance $d_h = 1$. The explicit expressions for k_R and k_D become very unwieldy with this mechanism. We restrict the analytical treatment to the most simple non-trivial case of $n = 2$. For cases with $n > 2$ we used Eq. (8) for numerical computation.

Concentrations of intermediates are now denoted by $[H_1] = [(ch)] = h_1$ and $[H_2] = [(hc)] = h_2$, and the kinetic differential equations are given by

$$\begin{aligned} \dot{c} &= -(k_{01} + k_{02}) c + k_{10} h_1 + k_{20} h_2 \\ \dot{h}_1 &= k_{01} c - (k_{10} + k_{13}) h_1 + k_{31} s \\ \dot{h}_2 &= k_{02} c - (k_{20} + k_{23}) h_2 + k_{32} s \\ \dot{s} &= k_{13} h_1 + k_{23} h_2 - (k_{31} + k_{32}) s. \end{aligned} \tag{14}$$

After elimination of h_1 and h_2 we find for the two over-all rate constants

$$\begin{aligned} k_R &= \frac{k_{01} k_{13} (k_{20} + k_{23}) + k_{02} k_{23} (k_{10} + k_{13})}{(k_{10} + k_{13})(k_{20} + k_{23})}, \\ k_D &= \frac{k_{10} k_{31} (k_{20} + k_{23}) + k_{20} k_{32} (k_{10} + k_{13})}{(k_{10} + k_{13})(k_{20} + k_{23})} \end{aligned} \tag{15}$$

which, of course, fulfill the equilibrium condition

$$K = \frac{k_R}{k_D} = \frac{k_{01}}{k_{10}} \cdot \frac{k_{13}}{k_{31}} = \frac{k_{02}}{k_{20}} \cdot \frac{k_{23}}{k_{32}}. \tag{16}$$

3. Estimation of rate constants

Rate constants of a chemical reaction ξ are, in the simplest case, related to activation energies by means of an Arrhenius law

$$k_\xi = A_\xi \cdot \exp\left\{-\frac{\Delta G_\xi^\ddagger}{RT}\right\}. \tag{17}$$

In order to actually compute the magnitude of the overall rate constants via Eq. (8), we need some assumptions concerning the individual rate constants $k_{\mu\varrho}$.

Each reaction involving two partially folded structures must have an equilibrium constant

$$K_{\mu\varrho} = \frac{k_{\mu\varrho}}{k_{\varrho\mu}}. \tag{18}$$

The corresponding change in free energy, $\Delta G_{\mu\varrho}$, is computed from the set of energy parameters used in the folding algorithm (Jaeger et al. 1989; Freier et al. 1986). For a calculation of the rate constants we partition the free energy into contributions resulting from both the folding and the melting process. This is done in accordance with experimental data reported by Pörschke (1974) for the folding kinetics of the oligoribonucleotide $A_6C_6U_6$ into a hairpin helix. The individual contributions are split as follows.

Let μ and ϱ be two structures which differ by a single stack which is present in ϱ but molten in μ. Thus the relevant structural state in ϱ consists of a stack of lengths s and the two flanking loops Λ_1 and Λ_2, of sizes λ_1 and λ_2, respectively. In μ this state turns into a large loop Λ of size $\lambda_1+\lambda_2+s$, according to the reaction path

$$\text{stack} + \Lambda_1 + \Lambda_2 \rightleftharpoons \Lambda_1 + \Lambda_2 \rightleftharpoons \Lambda, \tag{19}$$

with $\Lambda_1+\Lambda_2$ as the transition state. Let the destabilizing (positive) energy of a loop l be $\Delta G(l)$. The contribution from eliminating loop Λ is calculated from the energy tables underlying the folding procedure as:

$$\Delta G_{\mu\varrho}^{\text{loop}} = \Delta G(\Lambda_1) + \Delta G(\Lambda_2) - \Delta G(\Lambda). \tag{20}$$

(In the case of a stack that does not close an internal loop both Λ_2 and Λ are joints or free ends, whose free energy contributions are set to zero.) The contribution from the stack formation is denoted by $\Delta G_{\mu\varrho}^{\text{stack}}$, and is directly read off the energy tables.

The key assumption in estimating the rate constants is that along the reaction path (19) the absolute value of the stacking energy enters the rate constant of melting as the free energy of activation, $\Delta G_D^\ddagger$:

$$k_{\varrho\mu} = A_- \cdot \exp\left(-\frac{|\Delta G_{\varrho-\mu}^{\text{stack}}|}{RT}\right), \tag{21}$$

while the activation energy of recombination, $\Delta G_R^\ddagger$, is given by the change in loop energy:

$$k_{\mu\varrho} = A_+ \cdot \exp\left(-\frac{\Delta G_{\varrho-\mu}^{\text{loop}}}{RT}\right). \tag{22}$$

The rate constants determined by Pörschke for a loop of six bases at room temperature, $k_D = 2.6 \times 10^4\ \text{s}^{-1}$ and $k_R = 2.4 \times 10^4\ \text{s}^{-1}$ ($T = 24.2\,^\circ\text{C}$), serve as reference. The energy parameter set used here (Jaeger et al. 1989, Freier et al. 1986) yields $\Delta G^{\text{stack}} = -5.2$ kcal/mol and $\Delta G^{\text{loop}} = 5.1$ kcal/mol, and thus

$$A_+ = 1.35 \cdot 10^8 \quad \text{and} \quad A_- = 1.75 \cdot 10^8, \tag{23}$$

which agree within experimental error. We set $A = A_+ = A_-$. The effective overall activation energies then are simply given by

$$\Delta G_R^\ddagger = -RT \ln \frac{k_R}{A} \quad \text{and} \quad \Delta G_D^\ddagger = -RT \ln \frac{k_D}{A}. \tag{24}$$

Our calculations will refer to $\Delta G_R^\ddagger$ and $\Delta G_D^\ddagger$, since the over-all rate constants vary by more than 10 orders of magnitude (see also the Appendix).

4. Computational results

4.1. Dynamics

In this section we briefly discuss the melting dynamics by numerically integrating Eqs. (2) for the case of $tRNA^{Phe}$ from *E. coli*. The secondary structure of $tRNA^{Phe}$ is shown in Fig. 2a. It contains four stacks, labelled from 1 to 4 clockwise, with stack 4 being the acceptor stack. A configuration is a binary string of length four, with the leftmost position referring to stack 1 and the rightmost position to stack 4. Configuration chch, for example, indicates the presence of stacks 2 and 4, and the absence of stacks 1 and 3.

Figure 2b shows the dynamics at 37 °C starting from the linear form. The two structures, each consisting of one stack that closes the smallest hairpin loop, hccc and chcc, build up fastest. Formation of hairpin 3, cchc, is slightly slower, while ccch, leading to the largest loop, is negligible. Once a hairpin structure has formed, other hairpin components are added more easily than the closing of stack 4, since it now involves the formation of a more destabilizing internal loop. Hence from hccc, chcc and cchc the folding process leads to hhcc, chhc and hchc. The closing of stack 4 is now even more delayed, since it would involve formation of a multiloop whose free energy of formation is less favorable than other loop structures. Hence hhcc, chhc and hchc, all contribute to the build-up of hhhc. Finally the fully developed secondary structure, hhhh, is formed by closing the multiloop with stack 4.

Figure 2c shows the melting curve of $tRNA^{Phe}$ as the temperature dependence of the specific heat C, where $C = \mathrm{d}H/\mathrm{d}T$ and $H = kT^2\,\partial \ln Q/\partial T$ (McCaskill 1990). The partition function Q has been obtained using McCaskill's generalization of the dynamic programming algorithm for secondary structures (McCaskill 1990). The shoulder at about 45 °C is due to the opening of the multiloop closing stack 4. The rest of the structure melts at 68 °C. The kinetics of melting are shown in Fig. 2d for a temperature of 80 °C. The melting process begins with stack 4, and essentially reverses the sequence of the folding events. With rising temperature the stacking energy of stack 4 drops the most relative to the other stacks: it

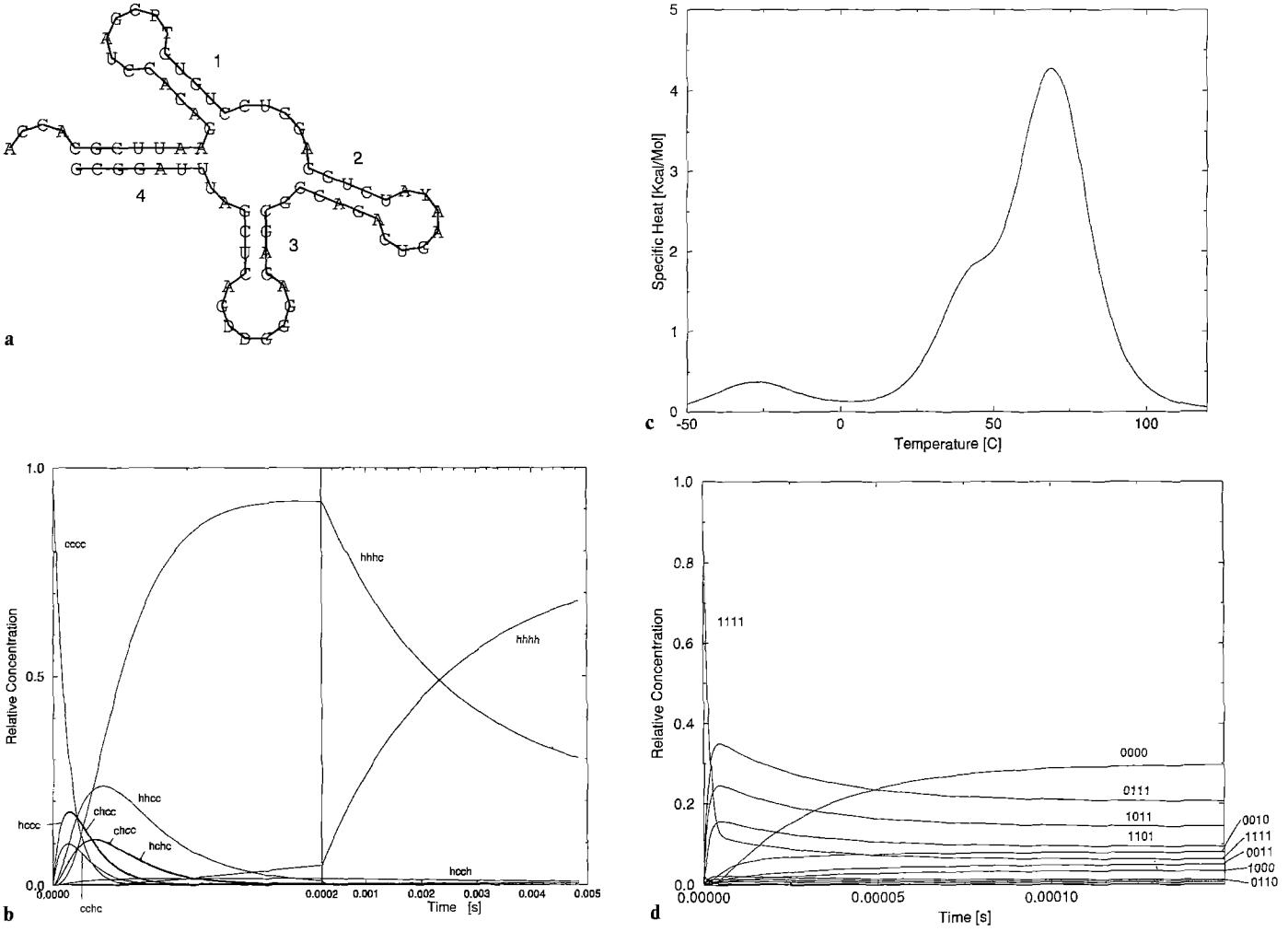

Fig. 2 a–d. Dynamics of refolding and melting of $tRNA^{Phe}$ from *E. coli*. **a** Minimum free energy structure. Each number indicates the position that refers to the corresponding stack in the binary encoding of the individual configurations. The leftmost position is 1, the rightmost is 4. **b** Refolding dynamics at 37 °C. **c** Melting curve computed via the partition function. **d** Melting dynamics at 80 °C. See text for details

therefore opens first, even if it is the longest paired region. The temperature at which the linear structure is dominant for the first time, 71.5 °C, agrees fairly well with the major peak at 68 °C in the computed melting curve.

$$\mathrm{C} \underset{k_{10}}{\overset{k_{01}}{\rightleftharpoons}} \mathrm{H}_1 \underset{k_{21}}{\overset{k_{12}}{\rightleftharpoons}} \mathrm{H}_{12} \underset{k_{32}}{\overset{k_{23}}{\rightleftharpoons}} \mathrm{H}_{123} \underset{k_{43}}{\overset{k_{34}}{\rightleftharpoons}} \cdots \underset{k_{m-1,m-2}}{\overset{k_{m-2,m-1}}{\rightleftharpoons}} \mathrm{H}_{12\ldots m-1} \underset{k_{m,m-1}}{\overset{k_{m-1,m}}{\rightleftharpoons}} \tag{9}$$

4.2. Comparison of sequential and hypercubic mechanism

The hypercubic melting model, Eq. (3), is solved numerically to calculate k_R and k_D. The vectors $(A^{-1}\boldsymbol{p})$ and $(A^{-1}\boldsymbol{q})$ are obtained from the linear system $A\boldsymbol{h}=\boldsymbol{p}$ and $A\boldsymbol{h}=\boldsymbol{q}$ by a Gaussian elimination scheme based on Crout's algorithm for the LU decomposition (Press et al. 1988, p. 43).

The sequential model strictly underestimates the rate constants. A comparison of the effective activation energies (Eq. (23)), $\Delta G_D^{\ddagger}$ and $\Delta G_R^{\ddagger}$, calculated for a sample of random sequences with both the sequential and the hypercubic mechanism is shown in Fig. 3. Although the differences are small, we chose the full hypercubic mechanism for all subsequent computations.

In the remaining sections we study the statistical structure of the landscapes that results from assigning to each sequence a $\Delta G_D^{\ddagger}$ and a $\Delta G_R^{\ddagger}$ at 37 °C according to our model.

4.3. Distribution of activation energies

Figure 4 shows that the average of $\Delta G_D^{\ddagger}$ increases linearly with the chain length n. The single most important contribution to k_D is likely to come from the most stable stack. We know that the average size of a stack rapidly becomes a constant as sequences grow longer, while the average number of stacks increases linearly with n (Fontana et al. 1993b). Hence the linear increase in $\Delta G_D^{\ddagger}$.

For a given length n, GC sequences form the most stable structures, GCXK sequences are less stable and

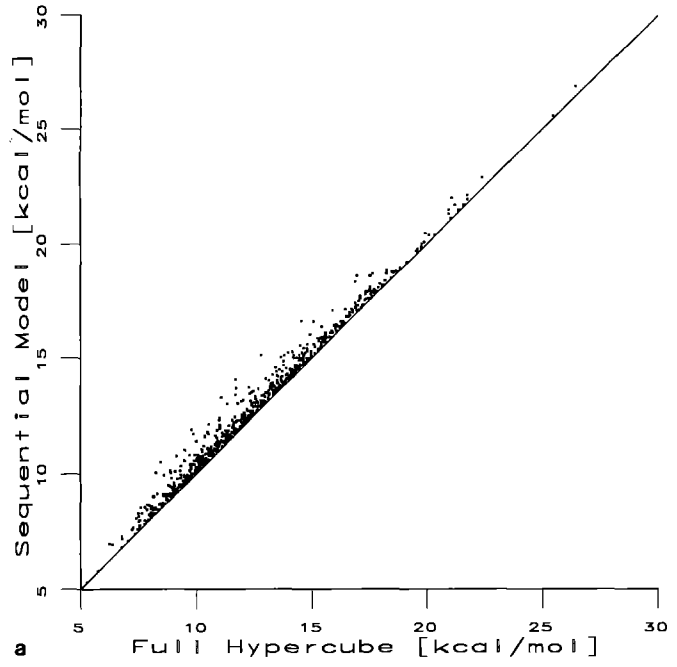

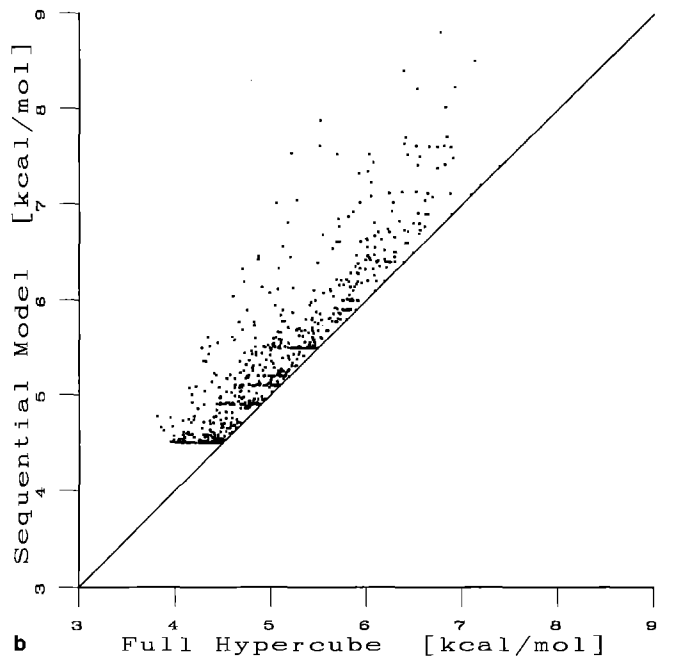

Fig. 3 a, b. Comparison of effective activation energies $\Delta G_D^{\ddagger}$ (r.h.s.) and $\Delta G_R^{\ddagger}$ (l.h.s.), as obtained from the sequential and the hypercubic melting mechanism

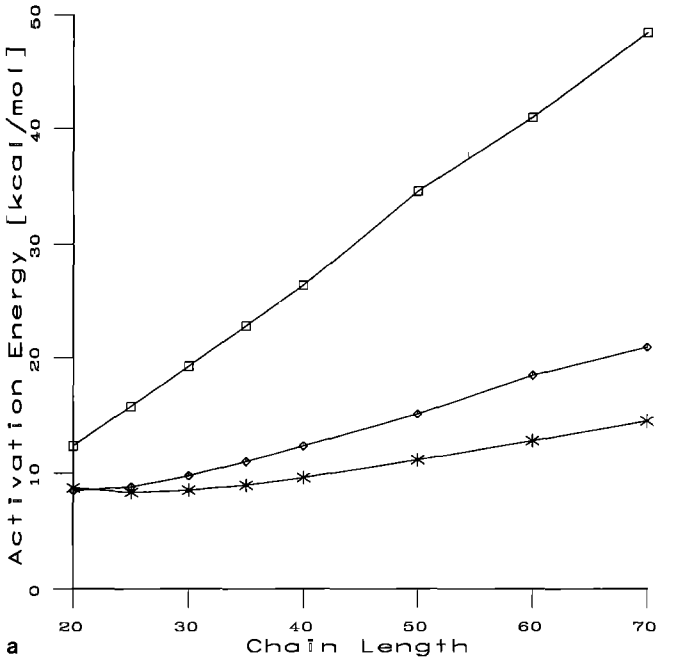

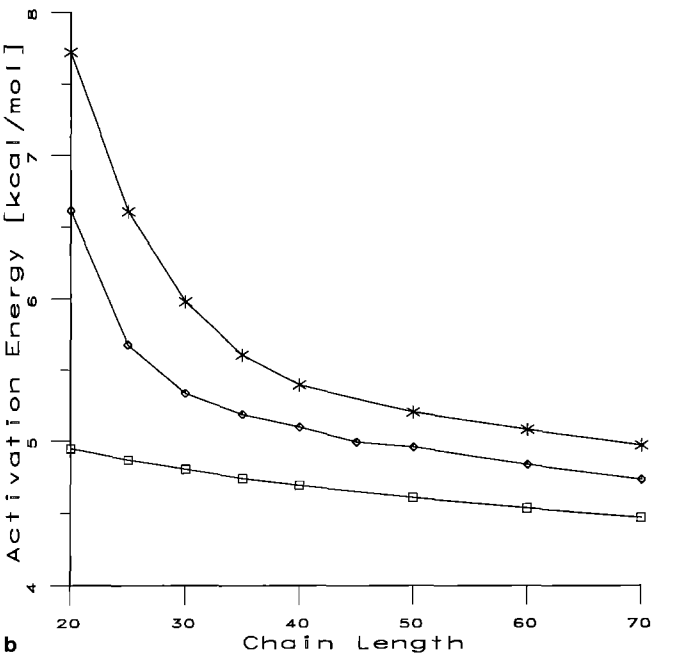

Fig. 4 a, b. Average activation energies for the dissociation (*top*) and the recombination reaction (*bottom*) as a function of the chain length. □, GC; ★, AUCG; ◇, GCXK

AUGC sequences are the most unstable. This fact is reflected in the dependence of $\Delta G_D^{\ddagger}$ on the chosen alphabet. For the GC alphabet the dissociation activation energies of longer chains are so large that the structures practically never open totally.

The average of $\Delta G_R^{\ddagger}$ (Fig. 4) tends towards a constant value for longer chains. This suggests that the rate limiting step for structure formation is the closing of the first hairpin loop (and there may be several parallel and equivalent paths for this). The loop formation energies enter $\Delta G_R^{\ddagger}$, and the average loop size becomes constant for long chains (Fontana et al. 1993 b). The alphabet dependence for the overall activation energy of recombination is reversed with respect to the melting (dissociation) case.

The distribution of activation energies is consistent with a Gaussian distribution for long chains (not shown). This behavior is to be expected since the individual structure elements contribute independently to the activation energies and the number of structure elements increases (linearly) with chain length (Fontana et al. 1993 b). For all alphabets the variance of $\Delta G_R^{\ddagger}$ decreases with n, whereas the variance of $\Delta G_D^{\ddagger}$ increases approximately linearly

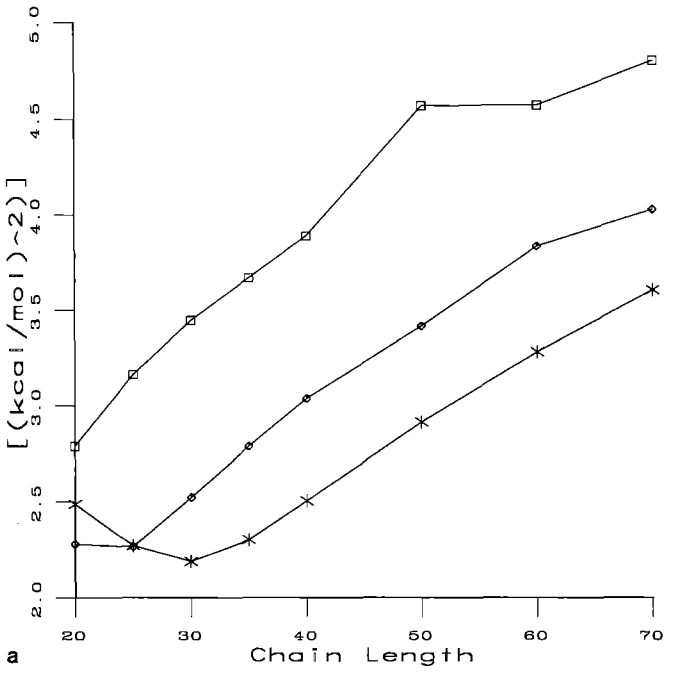

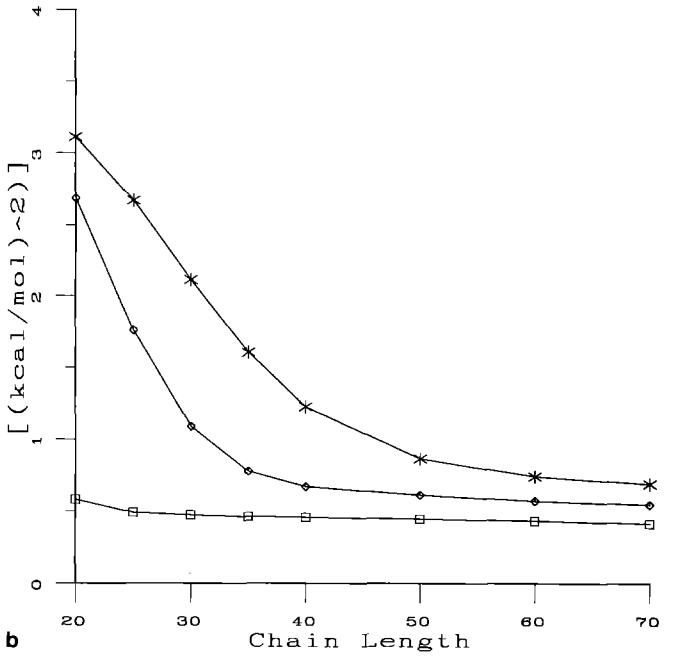

Fig. 5 a, b. Variances of the activation energies. □, GC; ★, AUCG; ◇, GCXK. *Upper part*: melting reaction, *lower part*: recombination reaction

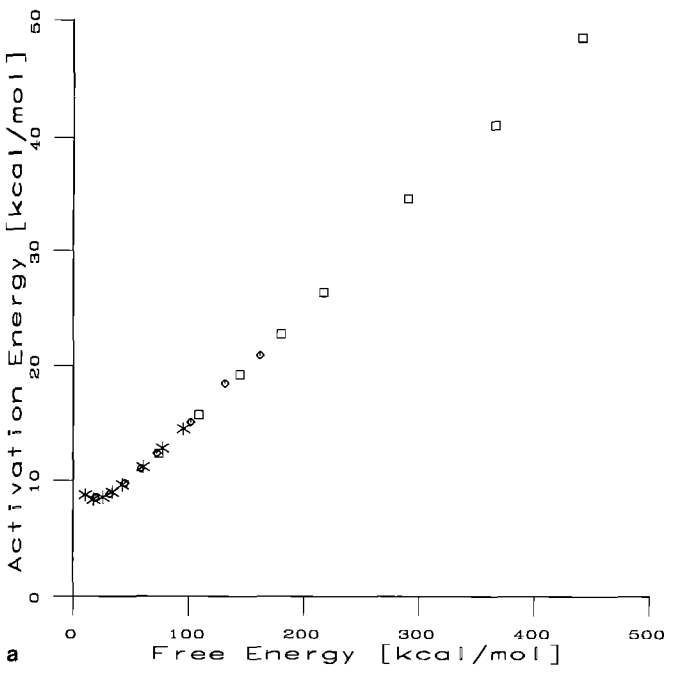

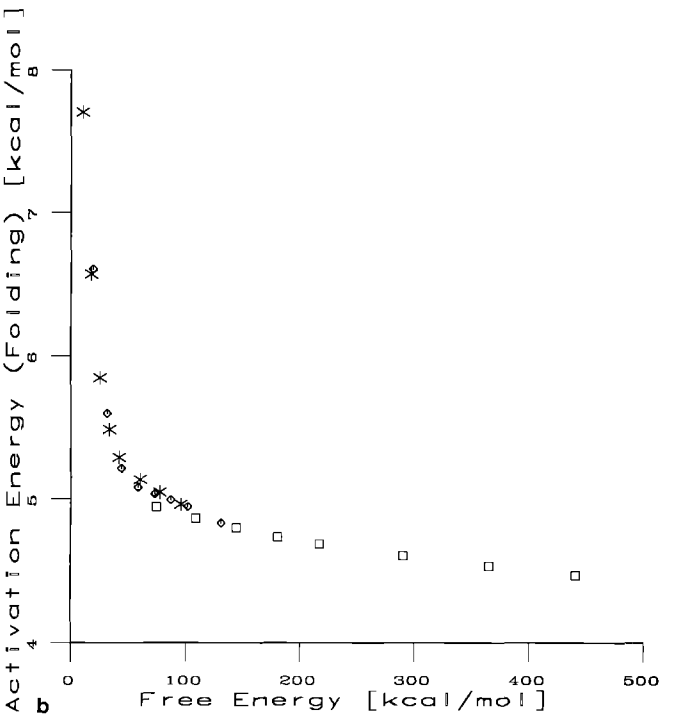

Fig. 6 a, b. Activation energies as function of the free energy of folding for the three different alphabets □, GC; ★, AUCG; ◇, GCXK. *Upper part*: melting reaction, *lower part*: recombination reaction

(Fig. 5). The distribution of free energies of activation for the recombination landscape, therefore, sharpens with increasing n.

The alphabet and chain length dependencies are exclusively due to the differences in the average structure stability they induce. This is seen in Fig. 6, where average activation energies of both recombination and dissociation are represented as a function of the average free energy of folding: the curves are independent of alphabet and chain length. The same holds for the variances (not shown).

4.4. Landscape correlation lengths

Landscapes that arise by assigning some property $f(x)$ to a configuration x can be characterized by their ruggedness (Kauffman and Levin 1987; Kauffman et al. 1988;

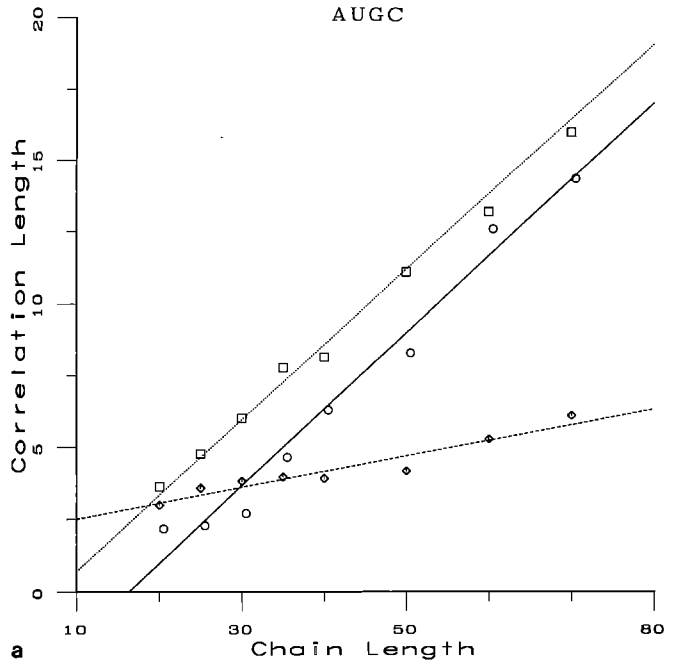

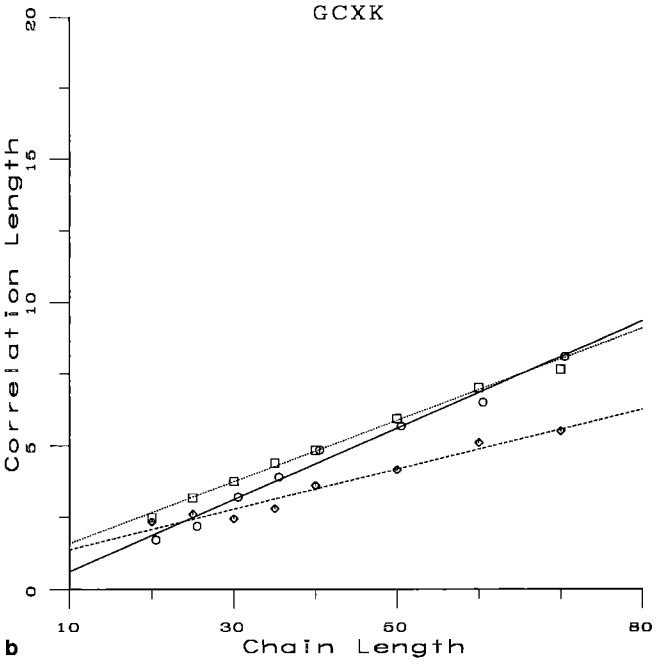

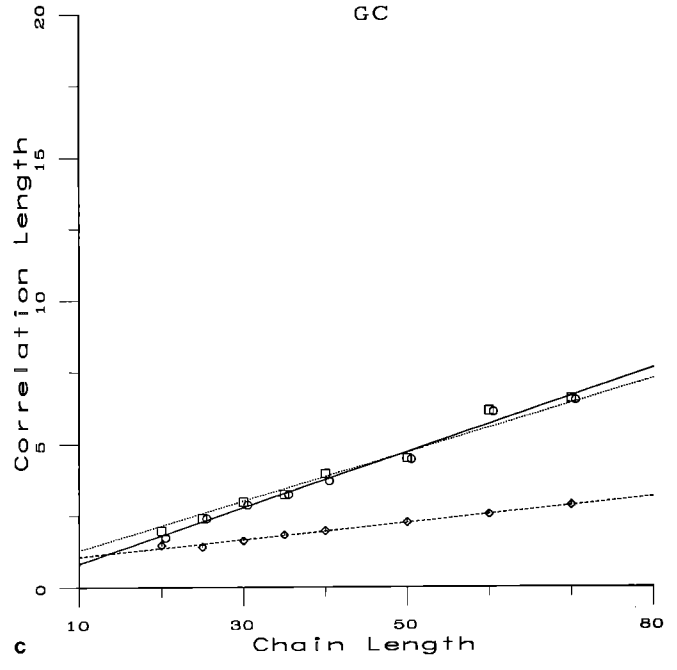

Fig. 7 a–c. Chain length dependence of correlation length. Free energy ΔG^0: □ and *dotted line*. Effective activation energy of melting $\Delta G_D^{\ddagger}$: ○ and *full line*. Effective activation energy of recombination $\Delta G_R^{\ddagger}$: ◇ and *dashed line*

Macken and Perelson 1989; Eigen et al. 1989; Weinberger 1990, 1991; Schuster 1991; Fontana et al. 1991, 1993a, b; Weinberger and Stadler 1992). This ruggedness can be conveniently quantified by means of a landscape correlation function

$$\varrho(d) = \frac{\langle f(x) f(y)\rangle_{d(x,y)=d} - \langle f\rangle^2}{\langle f(p) f(q)\rangle_{\text{random}} - \langle f\rangle^2}. \tag{25}$$

The averages $\langle . \rangle_{d(x,y)=d}$ refer to pairs of sequences with given Hamming distance d in sequence space, and $\langle . \rangle_{\text{random}}$ refers to a pair of sequences which are chosen independently at random. It has proven useful (Fontana et al. 1991) to characterize the autocorrelation function by a "correlation length" l defined by

$$\varrho(l) = 1/e \tag{26}$$

although $\varrho(d)$ is usually not a single decaying exponential.

The correlation lengths computed for both activation energy landscapes increase linearly with chain length n (see Fig. 7). The same behavior is observed for the correlation length of the free energy of structure formation (Fontana et al. 1993b). For all three alphabets the rate of increase is considerably smaller for the activation energy of recombination.

The AUGC alphabet has the highest correlation lengths for both activation energy landscapes; the GC alphabet has the smallest. This reflects the alphabet dependency in the stability of the secondary structures towards mutations in the underlying sequences. Independently of alphabet the correlation lengths of the $\Delta G_R^{\ddagger}$ landscapes are extremely short, indicating an almost uncorrelated landscape.

In agreement with Fig. 6 the $\Delta G_R^{\ddagger}$ landscape has a very weak dependence on chain length, suggesting once more that structure formation according to this model depends mostly on the first stack formation event.

5. Conclusions

We have presented a simple model for the kinetic melting (and refolding) behavior of RNA secondary structures. The model does not formalize a kinetic process of folding, or melting, that occurs on the space of all possible secondary structure configurations that are accessible to a given sequence. It rather assumes that the secondary structure is known beforehand by an independent calcu-

lation. It then considers only those processes that involve those structural elements that constitute the minimum free energy secondary structure. Nevertheless, in the case of $tRNA^{Phe}$ the melting point, as determined by the kinetic model, agrees remarkably well with an independently calculated melting curve that takes into account the entire equilibrium ensemble of structures for the sequence (Computations according to McCaskill 1990 and Bonhoeffer et al. 1993).

The average values and variances of the activation energies of both melting and refolding are seen to depend only on the average energy of the structures, independently of the alphabet used to build the sequences and independently of their chain length.

The average overall activation energy of refolding saturates to a constant, and its distribution sharpens for longer chains. This indicates that the rate limiting step is the formation of the first stack from the linear structure.

The correlation lengths for both activation energy landscapes scale linearly with chain length for all alphabets. The detailed scaling behavior of the "melting landscape" closely resembles the landscape of the free energy of structure formation investigated in earlier work. The correlation structure of the "recombination landscape" varies weakly with chain length, in agreement with the previous result indicating a nucleation event.

Acknowledgements. Useful discussions with Dipl. Phys. Ivo Hofacker and Dipl. Chem. Erich Bornberg-Bauer are greatefully acknowledged. This work was supported financially by the Austrian Fonds zur Förderung der Wissenschaftlichen Forschung, Project Nos. S5305-PHY and P8526-MOB.

Appendix

In this appendix we explain formally why we consider the landscape of activation energies rather than directly the landscape of rate constants. The informal reason is obvious: owing to the exponential relationship between activation energy and rate constants, the landscape of the latter will appear practically uncorrelated.

For the sake of simplicity we will assume that the pre-exponential factor A_ξ in Eq. (17) does not depend on the RNA sequence. We further assume that the $\Delta G^\ddagger$ landscape has a Gaussian distribution with correlation coefficients

$$\varrho(x,y)=\frac{\langle \Delta G^\ddagger(x)\,\Delta G^\ddagger(y)\rangle-\langle \Delta G^\ddagger\rangle^2}{\langle(\Delta G^\ddagger)^2\rangle-\langle \Delta G^\ddagger\rangle^2} \tag{A1}$$

where x and y denote fixed-length sequences. In view of our results in section 4.3 the Gaussian assumption is justified. In order to facilitate the subsequent calculations we will use the dimensionless variables

$$g_x=\frac{\Delta G^\ddagger(x)-\langle \Delta G^\ddagger\rangle}{\sqrt{\langle(\Delta G^\ddagger)^2\rangle-\langle \Delta G^\ddagger\rangle^2}}. \tag{A2}$$

The correlation coefficient remains unchanged by this linear transformation. From the assumption of a Gaussian distribution we obtained for the joint distribution

$$p(g_x,g_y)=\frac{1}{2\pi\sqrt{1-\varrho^2}}\cdot\exp\left\{-\frac{1}{2(1-\varrho^2)}\cdot(g_x^2-2\varrho\,g_x g_y-g_y^2)\right\} \tag{A3}$$

for any two sequences x and y (using the abbreviation $\varrho=\varrho(x,y)$), and

$$p(g)=\frac{1}{\sqrt{2\pi}}\exp\left(-\frac{1}{2}g^2\right). \tag{A4}$$

The correlation coefficient $\hat{\varrho}(x,y)$ of the corresponding rate constants is given by

$$\hat{\varrho}(x,y)=\frac{\langle k_x k_y\rangle-\langle k\rangle^2}{\langle k^2\rangle-\langle k\rangle^2}. \tag{A5}$$

This expression is evaluated by considering that the rate constant can be expressed as

$$k_x=B\cdot e^{q\cdot g_x}\quad\text{with}$$
$$B=A\cdot e^{\frac{\langle \Delta G^\ddagger\rangle}{RT}},$$
$$q=-\frac{\sqrt{\langle(\Delta G^\ddagger)^2\rangle-\langle \Delta G^\ddagger\rangle^2}}{RT}. \tag{A6}$$

From the Gaussian integrals

$$\begin{aligned}\langle k\rangle&=\int_{-\infty}^{+\infty}\frac{1}{\sqrt{2\pi}}\exp\left(-\frac{1}{2}g^2\right)\cdot B e^{qg}\,dg\\&=B e^{q^2/2}=B\sqrt{\alpha}\\\langle k^2\rangle&=\int_{-\infty}^{+\infty}\frac{1}{\sqrt{2\pi}}\exp\left(-\frac{1}{2}g^2\right)\cdot B^2(e^{qg})^2\,dg\\&=B^2 e^{2q^2}=B^2\alpha^2\end{aligned} \tag{A7}$$

$$\langle k_x k_y\rangle=\frac{B^2}{2\pi\sqrt{1-\varrho^2}}\int_{-\infty}^{+\infty}\exp\left\{-\frac{g_x^2-2\varrho\,g_x g_y-g_y^2}{2(1-\varrho^2)}\right\}\cdot e^{q(g_x+g_y)}\,dg_x\,dg_y=B^2\,e^{q^2(1+\varrho)}=B^2\,\alpha^{1+\varrho(x,y)}$$

and with the abbreviation

$$\alpha=e^{q^2}=\exp\left\{\frac{\langle(\Delta G^\ddagger)^2\rangle-\langle \Delta G^\ddagger\rangle^2}{(RT)^2}\right\} \tag{A8}$$

we obtain

$$\hat{\varrho}_\alpha(x,y)=\frac{\alpha^{\varrho(x,y)}-1}{\alpha-1}. \tag{A9}$$

The function $f(t)=\frac{\alpha^t-1}{\alpha-1}$ is concave for all t and all $\alpha>1$, i.e. all $T>0$, and furthermore $f(0)=0$ and $f(1)=1$. It follows immediately that

$$|\varrho(x,y)|>|\hat{\varrho}_\alpha(x,y)| \tag{A10}$$

for all $T>0$ whenever $\varrho(x,y)\neq\hat{\varrho}(x,y)=0$ or 1.

Let us assume that $\varrho(x,y)$ is only a function of the Hamming distance $d=d_H(x,y)$ between sequences x and

y. Suppose $\varrho(d)$ has a representation

$$\varrho(d) = 1 - \frac{1}{l} d + o(d) \tag{A11}$$

where l may be interpreted as a characteristic length scale. A simple calculation then shows that $\hat{\varrho}(d)$ may be represented as

$$\hat{\varrho}_\alpha(d) = 1 - \frac{1}{\hat{l}_\alpha} d + o(d) \tag{A12}$$

with the characteristic length scale on the landscape of rate constants given by

$$\hat{l}_\alpha = \frac{\alpha - 1}{\alpha \log \alpha} \cdot l. \tag{A13}$$

For large n the parameter α increases exponentially because

$$\langle \Delta G^{\ddagger})^2 \rangle - \langle \Delta G^{\ddagger} \rangle^2 \sim s^2 \cdot n \tag{A14}$$

and thus $\frac{\alpha - 1}{\alpha} \to 1$. We finally obtain

$$\hat{l}_\alpha \sim \left(\frac{RT}{s}\right)^2 \cdot \frac{l}{n}. \tag{A15}$$

In view of the results of Sect. 4.4, the correlation lengths for the activation energy landscapes considered here certainly obey the relation

$$l \leq \mathcal{O}(n) \tag{A16}$$

and, therefore, we expect that

$$\hat{l}_\alpha \leq \mathcal{O}(1) \tag{A17}$$

for any positive temperature T. We conclude that landscapes of reaction rate constants become essentially uncorrelated for long sequences.

References

Beaudry AA, Joyce GF (1992) Directed evolution of an RNA enzyme. Science 257:635–641

Bonhoeffer S, McCaskill JS, Stadler PF, Schuster P (1993) Temperature dependent RNA landscapes. A study based on partition functions. Eur Biophys J 22:13–24

Eigen M, McCaskill JS, Schuster P (1989) The molecular quasispecies. Adv Chem Phys 75:149–263

Ellington AD, Szostak JW (1990) In vitro selection of RNA molecules that bind specific ligands. Nature 346:818–822

Feinberg M (1977) Mathematical aspects of mass action kinetics. In: Lapidus L, Amundson NR (eds) Chemical reactor theory. Prentice Hall, Englewood Cliffs, NJ, pp 1–78

Fernández A, Shakhnovich EI (1990) Activation-energy landscape for metastable RNA folding. Phys Rev A 42:3657–3659

Fontana W, Griesmacher T, Schnabl W, Stadler PF, Schuster P (1991) Statistics of landscapes based on free energies replication and degradation rate constants of RNA secondary structures. Mh Chem 122:795–819

Fontana W, Konings DAM, Stadler PF, Schuster P (1993a) Statistics of RNA secondary structures. SFI preprint 92-02-007. Biopolymers (submitted for publication)

Fontana W, Stadler PF, Bornberg-Bauer EG, Griesmacher T, Hofacker IL, Tacker M, Tarazona P, Weinberger ED, Schuster P (1993b) Phys Rev E47:2083–2099

Freier SM, Kierzek R, Jaeger JA, Sugimoto N, Caruthers MH, Neilson T, Turner DH (1986) Improved free-energy parameters for predictions of RNA duplex stability. Biochemistry 83:9373–9377

Horowitz MSZ, Dube DK, Loeb LA (1989) Selection of new biological activities from random nucleotide sequences. Genome 31:112–117

Jaeger JA, Turner DH, Zuker M (1989) Improved predictions of secondary structures for RNA. Biochemistry 86:7706–7710

Joyce GF (1989) Amplification, mutation and selection of catalytic RNA. Gene 82:83–87

Kauffman SA, Levin S (1987) Towards a general theory of adaptive walks on rugged landscapes. J. Theor Biol 128:11–45

Kauffman SA, Weinberger ED, Perelson AS (1988) Maturation of the immune response via adaptive walks on affinity landscapes. Theoretical immunology, Part I, Santa Fe Institute Studies in the Sciences of Complexity. Perelson AS (ed), Addison-Wesley, Reading, Mass

Macken CA, Perelson AS (1989) Protein evolution on rugged landscapes. Proc Nat Acad Sci 86:6191–6195

McCaskill JS (1990) The equilibrium partition function and base pair binding probabilities for RNA secondary structures. Biopolymers 29:1105–1119

Peritz AE, Kierzek R, Sugimoto N, Turner DH (1991) Thermodynamic study of internal loops in oligoribonucleotides: symmetric loops are more stable than asymmetric loops. Biochemistry 30:6428–6436

Piccirrilli JA, Krauch T, Moroney SE, Brenner SA (1990) Enzymatic incorporation of a new base pair into DNA and RNA extends the genetic alphabet. Nature 343:33–37

Pörschke D (1971) Cooperative nonenzymic base recognition II. Thermodynamics of the helix-coil transition of oligoadenylic+oligouridylic acids. Biopolymers 10:1989–2013

Pörschke D (1974) Thermodynamic and kinetic parameters of an oligonucleotide hairpin helix. Biophys Chem 1:381–386

Pörschke D, Eigen M (1971) Co-operative non-enzymic base recognition III. Kinetics of the oligoribouridylic-oligoriboadenylic acid system and of oligoriboadenylic acid alone at acidic pH. J Mol Biol 62:361–381

Press WH, Flannery BP, Teukolsky SA, Vetterling WT (1988) Numerical recipes. Cambridge University Press, New York

Schuster P (1991) Complex optimization in an artificial RNA world. In: Farmer D, Langton C, Rasmussen S, Taylor C: Artificial Life II, SFI Studies in the Science of Complexity XII. Addison-Wesley, Reading, Mass

Stadler PF, Happel R (1992) Correlation structure of the landscape of the graph-bipartitioning-problem. J Phys A: Math Gen 25:3103–3110

Stadler PF, Schnabl W (1992) The landscape of the travelling salesman problem. Phys Lett A161:337–344

Tuerk CTC, Gold L (1990) Systematic evolution of ligands by exponential enrichment: RNA ligands to bacteriophage T4 DNA polymerase. Science 249:505–510

Waterman MS, Smith TF (1978) RNA secondary structure: a complete mathematical analysis. Math Biosci 42:257–266

Weinberger ED (1990) Correlated and uncorrelated fitness landscapes and how to tell the difference. Biol Cybern 63:325–336

Weinberger ED (1991) Local properties the $N-k$ model, a tuneably rugged energy landscape. Phys Rev A 44:6399–6413

Weinberger ED, Stadler PF (1992) Why some fitness landscapes are fractal. J Theor Biol (submitted for publication)

Zuker M (1989) The use of dynamic programming algorithms in RNA secondary structure prediction. In: Waterman MS, Mathematical methods for DNA sequences. CRC Press, Boca Raton

Zuker M, Stiegler P (1981) Optimal computer folding of large RNA sequences using thermodynamic and auxiliary information. Nucl Acid Res 9:133–148

Zuker M, Sankoff D (1984) RNA secondary structures and their prediction. Bull Math Biol 46:591–621